HHS Public Access

Author manuscript

Nat Neurosci. Author manuscript; available in PMC 2011 October 01.

Published in final edited form as:

Nat Neurosci. 2011 April ; 14(4): 487–494. doi:10.1038/nn.2775.

Presynaptic CLC-3 Determines Quantal Size of Inhibitory Transmission in the Hippocampus

Vladimir Riazanski[*], **Ludmila V. Deriy**[*], **Pavel D. Shevchenko**, **Brandy Le**, **Erwin A. Gomez**, and **Deborah J. Nelson**

Department of Neurobiology, Pharmacology and Physiology, The University of Chicago, Chicago, IL 60637

Abstract

The absence of the chloride channel CLC-3 in *Clcn3*$^{-/-}$ mice results in hippocampal degeneration with a distinct temporal-spatial sequence reminiscent of neuronal loss in temporal lobe epilepsy. We examined how the loss of CLC-3 might impact GABAergic synaptic transmission in the hippocampus. An electrophysiological study of synaptic function in *Clcn3*$^{+/+}$ and *Clcn3*-$^{-/-}$ mice in hippocampal slices before the onset of neurodegeneration, revealed a significant decrease in the amplitude and frequency of mIPSCs. We found that CLC-3 colocalizes with the vesicular GABA transporter VGAT in the CA1 region of the hippocampus. Cl^--induced acidification of inhibitory synaptic vesicles showed a significant dependence on CLC-3 expression. The decrement in inhibitory transmission in the *Clcn3*$^{-/-}$ animals suggests a decrease in neurotransmitter loading of synaptic vesicles which we attributed to defective vesicular acidification. Our observations extend the role of Cl^- in inhibitory transmission from that of a postsynaptic permeant species to a presynaptic regulatory element.

CLC-3 chloride channels, members of an extended family of voltage-gated chloride channels and transporters, are ubiquitously expressed throughout the brain. The CLC-3 knockout (*Clcn3*$^{-/-}$) mouse shows complete postnatal neurodegeneration of the hippocampus 1–3 with a temporal-spatial sequence which would suggest a strong relationship to network connectivity 2. The hippocampal formation appears normal up to and including the fourth postnatal week in development indicating that *Clcn-3*$^{-/-}$ animals are capable of generating a properly structured central nervous system. Loss of hippocampal neurons becomes evident by postnatal week 12 with the most severe decrement observed in the dentate gyrus and CA1 2. By twelve months of age, total degeneration of the hippocampal formation occurs with the progressive enlargement of the lateral ventricles. The profound and developmentally delayed neuronal degeneration observed in the

Corresponding author: Deborah J. Nelson, The University of Chicago, Department of Neurobiology, Pharmacology and Physiology, 947 E. 58th St., Chicago, IL 60637, nelson@uchicago.edu, Tel: 773-702-0126, FAX: 773-834-4522.

*These authors contributed equally to this work.

AUTHOR CONTRIBUTIONS

V.R., L.D., and D.N. designed the project, analyzed the data and wrote the manuscript. V.R, L.D., P.S., B.L., and E.G. performed the experiments.

Clcn-3$^{-/-}$ animals provides a unique tool to examine the physiological role of CLC-3 in brain maturation.

CLC-3 channels are localized at both pre- and postsynaptic sites, thereby providing a new and important level of regulation in the modulation of synaptic plasticity. Presynaptically, CLC-3 has been localized to synaptic vesicles where it has been suggested that the channel contributes to both synaptic vesicle pH regulation and transmitter filling1, 4, 5. This hypothesis, at least in the glutamatergic system, remains controversial 6. Postsynaptically, CLC-3 channels have been localized to glutamatergic synapses in the hippocampus where they augment synaptic efficacy as a function of changes in postsynaptic Cl^- homeostasis 4. As determinants of cell function, an enhancement of CLC-3 expression during cell division has recently demonstrated that the channel is essential to both normal and malignant glial cell division 7 and migration 8.

Our studies are targeted at an integrated understanding of the role CLC-3 plays in the fundamental aspects of hippocampal neuronal excitability. Localization of the channel in hippocampal slices at perisomatic inhibitory synapses in CA1 neurons suggested that the early observations of Dickerson and colleagues 2 implicating deficiencies in CLC-3 expression to changes in GABA-ergic signaling in the forebrain might contribute to the early stages of neurodegeneration. To assess a physiological role for ClC-3 in inhibitory transmission, we began by undertaking a comparison of inhibitory activity in hippocampal brain slices from CLC-3-deficient animals prior to observable neurodegeneration and slices from the *Clcn3*$^{+/+}$ mouse brain. Preparations from *Clcn3*$^{-/-}$ mice demonstrated a significant decrease in miniature IPSC frequency and quantal size suggesting a distinct presynaptic CLC-3 dependent regulatory mechanism.

Previous studies carried out on the purified, reconstituted vesicular inhibitory amino acid transporter (VGAT) have suggested that the inhibitory transmitter GABA is co-transported into proteoliposomes with two equivalents of external Cl 9. To determine whether CLC-3 expressed in inhibitory synaptic vesicles provides a parallel Cl^- entry pathway, we examined immunoisolated inhibitory vesicles from *Clcn3*$^{-/-}$ and *Clcn3*$^{+/+}$ animals. In addition, we created a rat model for the *Clcn3*$^{-/-}$ vesicles in order to circumvent possible neurodegenerative changes in transporter protein expression seen in the *Clcn3*$^{-/-}$ mice. Indeed, CLC-3 enhanced vesicle acidification rate and amplitude, supporting a presynaptic role for ClC-3 in the regulation of quantal size at inhibitory synapses.

RESULTS

Co-localization of CLC-3 with VGAT at hippocampal synapses

Immunohistochemistry on slice preparations in the CA1 *stratum pyramidale* revealed a prominent, punctate pattern of perisomatic CLC-3 staining (Fig. 1a). Since most of the perisomatic innervation of CA1 hippocampal pyramidal cells is derived from inhibitory synapses 10 and the fact that CLC-3 is expressed in synaptic vesicles 1, 4, we compared CLC-3 and VGAT immunoreactivity in hippocampal slices. Confocal, double-labeling studies demonstrated less profound expression in the *stratum radiatum* and *stratum oriens* (Fig.1b), with a high degree of overlap between anti-VGAT staining (Fig. 1c) and CLC-3

with a correlation coefficient of 0.92 as seen in the merged images in Fig. 1d–e. A similar degree of overlap existed between CLC-3 and VGLUT1; however, in contrast to that seen with VGAT, the overlap was concentrated in the *stratum radiatum* and *stratum oriens* (see Supplemental Figure S1 and Supplemental Table S1).

High levels of expression of CLC-3 at synaptic sites and the limits of resolution of light microscopy made it difficult to localize CLC-3 to synaptic vesicles as suggested by the co-localization with VGAT. In order to further compartmentalize its subsynaptic location/expression, we carried out subcellular fractionation of whole rat brains 21. The population of crude synaptic vesicles (CSV) appeared homogeneous in electron microscopy (Fig. 2a) and within the size range described elsewhere for synaptic vesicles 11. VGAT positive vesicles were immunopurified using anti-VGAT coated microbeads and examined in immuno-electron microscopy. Beads were stained with anti-CLC-3 followed by secondary antibody conjugated to 15 nm gold particles (Fig. 2b). As seen in the inserts in Fig. 2b, we observed CLC-3 localized to the bound, immuno-purified inhibitory synaptic vesicles.

Reduced miniature IPSC quantal size in Clcn3$^{-/-}$ mice

Next we tested whether the absence of CLC-3 expression at inhibitory synaptic terminals results in changes in synaptic transmission in the CA1 region of acute hippocampal slices from *Clcn3*$^{-/-}$ as compared to *Clcn3*$^{+/+}$ animals. We used animals between P18 and P25 without detectable neurodegeneration in the ventral part of the hippocampus. We pharmacologically isolated and analyzed miniature inhibitory currents (mIPSCs) as summarized in Fig 3. There was a significant reduction in both mIPSC frequency (Fig. 3a and b) as well as amplitude (Fig. 3c,d) in slices from *Clcn3*$^{-/-}$ animals as compared to *Clcn3*$^{+/+}$. The cumulative distribution of mIPSC amplitudes was significantly shifted toward smaller events in *Clcn3*$^{-/-}$ as compared to control (Fig. 3d). Currents recorded in slices from *Clcn3*$^{-/-}$ mice were significantly lower in amplitude as compared to currents from *Clcn3*$^{+/+}$ slices (see insert showing comparative box plot analysis in Fig. 3d). The detected difference in frequency and size of inhibitory events as a function of CLC-3 expression supports a role for vesicular CLC-3 in determining quantal size.

TRIS buffering reduces evoked IPSC amplitude—A decrease in mIPSC amplitude in the absence of CLC-3 could be due to attenuated vesicle reacidification and, therefore, neurotransmitter refilling. In order to investigate this possibility, we recorded evoked inhibitory post-synaptic currents in acute *Clcn3*$^{+/+}$ slices in the presence of 20 and 50 mM TRIS buffer. It has previously been shown that extracellularly added pH buffers are engulfed during recycling of synaptic vesicles following release 12, 13. Such TRIS loading of synaptic vesicles in cultured hippocampal neurons reduces the rate of vesicle reacidification 14, thereby, modeling the reduction of inhibitory synaptic transmission seen in the *Clcn3*$^{-/-}$ animal. In our experiments in slices from *Clcn3*$^{+/+}$ mice, we observed fast inhibition of evoked IPSCs with a stimulation frequency of 0.2 Hz that was dependent upon the TRIS concentration. In Fig. 4a, evoked inhibitory currents in the presence of increasing extracellular concentrations of TRIS are superimposed. Repetitive stimulation (Fig. 4b) shows rapid current inhibition in the presence of 50 mM TRIS and recovery upon TRIS removal from the bath. We reasoned that if synaptic vesicles from *Clcn3*$^{-/-}$ animals are

more alkaline than their *Clcn3*$^{+/+}$ counterparts, the magnitude of the TRIS- induced inhibition in the *Clcn3*$^{-/-}$ neurons should be exaggerated compared to responses from the *Clcn3*$^{+/+}$ neurons. Results of these experiments are depicted in Fig. 4c and data along with the concentration dependence of the TRIS-induced inhibition summarized in Fig. 4d.

If the changes seen in mIPSCs recorded from *Clcn3*$^{-/-}$ cells are due to reduced acidification and refilling, we would expect similar changes in mIPSC size in the presence of TRIS. In contrast to the fast inhibition observed for the evoked IPSC amplitude, addition of TRIS produced mIPSC amplitude inhibition with a significant lag time. We observed a decrease in mIPSC amplitude 20–30 min following the addition of TRIS (Fig. 4e–f). In that that the events are spontaneous, this process should occur with a lag time as reserve vesicles are released; however, following release, most or all of the recycling vesicles will be filled with TRIS. Similar to *Clcn3*$^{-/-}$ mIPSC amplitudes, we observed a left shift in the peak amplitude histogram as well as cumulative probability curve for the events recorded in the presence of TRIS (Fig. 4g). However, unlike data obtained with *Clcn3*$^{-/-}$ cells, we did not observe a significant decrease in event frequency in the presence of TRIS (Fig. 4h).

To rule out the possibility that changes in postsynaptic GABA receptor density were responsible for the decrease in mIPSC amplitude, we carried out experiments examining the response to brief puff applications of 10 μM GABA to the cell soma. The applications did not reveal a significant difference in the amplitude of evoked GABA-ergic currents between *Clcn3*$^{+/+}$ and *Clcn3*$^{-/-}$ neurons (Supplemental Fig. 2).

Slice preparations from *Clcn3*$^{+/+}$ and *Clcn3*$^{-/-}$ animals differed significantly in the level of apparent paired pulse depression (PPD) with the *Clcn3*$^{-/-}$ cells showing a diminished PPD (Supplemental Fig. 3a and b). In paired pulse experiments, there is a balance between two processes: depletion of the readily releasable vesicle pool during the first pulse and Ca^{2+} dependent facilitation of release during the second pulse. Changes in PPD, the ratio of second pulse amplitude to that of the first pulse could reflect a reduction in the amplitude and, therefore, release probability during the first pulse. Indeed, the IPSCs evoked with identical stimulation intensities induce larger responses in the *Clcn3*$^{+/+}$ than in *Clcn3*$^{-/-}$ or *Clcn3*$^{+/+}$ slices treated with 20 mM TRIS. (Supplemental Fig. 3c and d). In *Clcn3*$^{+/+}$ animals, PPD could be converted to the diminished responses similar to that seen in the *Clcn3*$^{-/-}$ slices in the presence of high extracellular TRIS (Supplemental Fig. S3a and b). These data suggested that the responses in the *Clcn3*$^{-/-}$ slices might be due to aberrant vesicle acidification and availability of refilled vesicles in the readily releasable pool during rapid recycling. Similar evoked current conversions, albeit in the absence of TRIS, have been observed in the studies of Kerr et al. in synaptotagmin 1 deficient mice 15. Given the PPD data coupled with the observations in Fig. 4, we undertook experiments that would allow us to compare Cl^--dependent acidification in synaptic vesicles isolated from *Clcn3*$^{+/+}$ and *Clcn3*$^{-/-}$ animals directly.

Inhibitory Clcn3$^{-/-}$ synaptic vesicles show reduced acidification—Our electrophysiological studies strongly suggested that a reduction in CLC-3 expression presents as a reduction in pre-synaptic function at inhibitory synapses, possibly dysfunctional loading of synaptic vesicles with the neurotransmitter. Neurotransmitter

loading is directly proportional to H^+ electrochemical gradient established by the vesicular ATPase (V-ATPase) and assayed *in vitro* as a change in the level of vesicle acidification 16. We compared acidification amplitude and rates between CSV isolated from *Clcn3*$^{+/+}$ and *Clcn3*$^{-/-}$ animals as a function of increasing [Cl^-] (Fig. 5a–c). External Cl^- enters the vesicle to neutralize the potential gradient set up by V-ATPase, thereby allowing further vesicle acidification. Although the magnitude of acidification did not differ between *Clcn3*$^{+/+}$ and *Clcn3*$^{-/-}$ CSV (Fig. 5a), the rate of acidification was significantly different and a function of Cl^- concentration (Fig. 5b).

In that the CSV population is composed primarily of excitatory, glutamatergic vesicles, we reasoned that vesicle subset selection was necessary to ascertain whether inhibitory vesicle acidification was more sensitive to CLC-3 expression. We designed a strategy to immuno-purify inhibitory vesicles, thus allowing subset comparison of *Clcn3*$^{-/-}$ and *Clcn3*$^{+/+}$ GABAergic vesicle acidification. The enriched inhibitory synaptic vesicle fraction was obtained by removing VGLUT1-positive synaptic vesicles from the CSV suspension using magnetic beads coated with anti-VGLUT1 antibodies. VGAT enrichment of this fraction was confirmed by Western blot analysis (Fig. 5d). Henceforth, we will refer to this fraction as inhibitory synaptic vesicles. Cl^--dependent acidification was compared between the *Clcn3*$^{+/+}$ and *Clcn3*$^{-/-}$ inhibitory vesicle fraction as well as the *Clcn3*$^{+/+}$ inhibitory synaptic vesicle fraction depleted of CLC-3 (Fig. 5e). The magnitude of acidification was significantly larger in *Clcn3*$^{+/+}$ inhibitory vesicles over that observed for the *Clcn3*$^{-/-}$ inhibitory vesicles. Inhibitory vesicles isolated from *Clcn3*$^{-/-}$ mice showed Cl^--dependent levels of acidification identical to that obtained using *Clcn3*$^{+/+}$ inhibitory vesicles depleted of CLC-3 providing further validation for the immuno-purification technique. Characterization of the degree of vesicle depletion/enrichment was confirmed by immunoblot analysis (Fig. 5d–f).

Immunoisolated rat synaptic vesicles mimic Clcn3$^{+/+}$ and Clcn3$^{-/-}$ vesicles— Although a functional comparison of inhibitory vesicles isolated from *Clcn3*$^{-/-}$ and *Clcn3*$^{+/+}$ animals showed a significant difference in the levels of acidification, further studies were limited not only by the number of age matched *Clcn3*$^{-/-}$ animals necessary for inhibitory vesicle immuno-purification, but also by the hippocampal neurodegenerative process in the *Clcn3*$^{-/-}$ mice which has been observed to decrease neurotransporter expression as well as vesicle number over time 6. In light of this fact, coupled with the possibility that *Clcn3*$^{-/-}$ animals might develop alternative Cl^- influx pathways to compensate for the loss of CLC-3 expression, we developed a rat model where we could study immuno-purified inhibitory vesicles depleted of CLC-3 as well. VGLUT1 depletion and VGAT enrichment of immunoisolated rat synaptic vesicles was confirmed by Western blotting (Fig. 6a). Cl^--dependent acidification profiles for excitatory (VGAT-depleted) and inhibitory (VGLUT1-depleted) synaptic vesicles in the presence of constant 10 mM glutamate or GABA, respectively, are compared in Fig. 6b. These data demonstrate that the magnitude of excitatory vesicle acidification is significantly greater in comparison to that observed for inhibitory vesicle fractions and, in part, dependent upon the presence of glutamate. We found that immuno-purified excitatory synaptic vesicles acidify in the presence of 10 mM glutamate even in the absence of Cl^- in the extravesicular milieu (Fig.

6b). This is in contrast to data from CSVs reported previously where low levels of Cl^- are suggested to be necessary to allosterically prime glutamate-induced acidification 6, 17. The concentration dependent [Cl^-]-induced change in the level of acidification in enriched excitatory and inhibitory subsets of vesicles is summarized in Fig. 6c. Inhibitory vesicle acidification showed only a weak [Cl^-]-dependence, even in the presence of transmitter, in comparison to that observed for VGLUT1-enriched vesicles. Comparative rates of acidification as a function of Cl^- are compared between the two synaptic vesicle populations in Fig. 6d. The rate of glutamate-induced acidification in the absence of Cl^- is significantly slower than in the presence of even low levels of Cl^-. VGAT-enriched vesicle acidification rates were slower than the excitatory vesicle population throughout the Cl^- concentration range; however, neither vesicle population showed a significant change in the rate of acidification as a function of increasing Cl^-. This implies that the acidification rate is likely to be set by V-ATPase turnover which is relatively constant and independent of an increase in the extravesicular Cl^- concentration gradient.

Inhibitory vesicles were depleted of CLC-3 using magnetic beads coated with anti-CLC-3 antibody as described above and were examined in acidification experiments in Fig. 7. The degree of CLC-3 depletion performed on enriched fractions of inhibitory synaptic vesicles was confirmed by Western blotting (Fig. 7a). A comparison of the Cl^--dependent acidification profiles for inhibitory vesicles expressing and depleted of CLC-3 matched that obtained for vesicles isolated from *Clcn3*$^{+/+}$ and *Clcn3*$^{-/-}$ animals (Fig. 5c) providing further validation for the rat model. Representative individual traces of acidification in Fig. 7b demonstrate a striking difference in the levels of acidification of inhibitory vesicles depending on the presence of CLC-3. The amplitude of acidification of inhibitory synaptic vesicles is significantly larger and is more Cl^--dependent in the presence of CLC-3 than in the CLC-3 depleted population, especially at higher [Cl^-] as shown by analysis of the data in Fig. 7c. The rate of inhibitory vesicle acidification in the presence of CLC-3 was not significantly different from that seen in the CLC-3-depleted fraction at all [Cl^-] (data not shown). Thus, although CLC-3 does not seem to alter the time constant describing the acidification process, it has a profound effect on the magnitude of acidification. These data demonstrate that CLC-3 has a strong impact on amplitude of acidification of inhibitory synaptic vesicles changing both vesicle filling and probability of release.

DISCUSSION

We have shown that the channel protein CLC-3 determines inhibitory synaptic strength presynaptically through alterations in the magnitude of acidification in VGAT-expressing inhibitory vesicles. CLC-3 is present in VGAT-expressing vesicles localized to perisomatic regions in the CA1 region of the hippocampus where we focused our electrophysiological studies. Expression of CLC-3 enhanced IPSC quantal size, leading us to hypothesize that expression of CLC-3 might enhance inhibitory transmission by regulating quantal content. Vesicle acidification, studied most prominently in glutamatergic excitatory vesicles, is Cl^- dependent and driven by the activity of the vesicular H^+-ATPase (see review 16). Our co-localization data show (Supplemental Fig. S1) that CLC-3 is present on VGLUT1 containing vesicles as well, which is in good agreement with a recent proteomic study of synaptic vesicles in which the relative levels of CLC-3 in glutamatergic and GABAergic vesicles

were found to be comparable 18. CLC-3 has been examined as a conductance pathway facilitating vesicle acidification, and thereby filling, at excitatory synapses 1, 6. Recent data in the literature suggest that VGLUT1 provides a parallel vesicular Cl^- shunt pathway ensuring efficient and rapid acidification/transmitter filling 6. In our experiments, acidification profiles in CSV from *Clcn-3*$^{+/+}$ and *Clcn-3*$^{-/-}$ animals showed no significant difference in the magnitude of acidification, a subject of controversy in the literature 1, 6, although the rate of acidification differed as a function of CLC-3 expression at low extravesicular Cl^- concentrations (Fig. 5b).

The CSV pool is made up predominantly of glutamatergic vesicles, thus obscuring data from the minority populations contributed by GABAergic, cholinergic and dopaminergic vesicles. Our experimental goal was then to measure acidification directly in immunoisolated, subset selected synaptic vesicles targeting VGAT-expressing vesicles. Antibody–coated beads have been used previously to examine both neurotransmitter uptake and acidification in synaptic vesicles 11. In these studies, the acidification levels obtained in the VGAT-isolated bead fraction were significantly lower than observed for the vesicles from the synaptophysin-isolated beads (presumably, primarily VGLUT1 positive). We reasoned that this reduction in acidification observed in VGAT positive vesicles could have been a consequence of antibody binding to the transporter itself during the isolation process, thereby, inhibiting function. In order to avoid this possibility in our experiments, we developed a negative selection strategy whereby we enriched the subset of interest, thus circumventing possible antibody-induced inhibitory effects on transporter function. Our immuno-enriched VGLUT1-depleted vesicles (inhibitory population) also showed a significant decrement in acidification levels over that seen in VGLUT1-enriched vesicle (excitatory vesicles) populations (Fig.6c) as that seen in the positive-selection bead studies 11. Both populations of vesicles, inhibitory and excitatory, show [Cl^-] dependent acidification, implying a general role for a Cl^- influx pathway in the acidification filling process.

Comparison of acidification magnitude and time course of inhibitory vesicles in both the mouse experiments and the rat model lacking CLC-3 confirmed that CLC-3 expression provides a significant contribution to the necessary Cl^- influx during vesicle acidification and filling. The immunoisolated VGAT-enriched vesicles depleted of CLC-3 showed a significant loss of acidification in the presence of increasing concentrations of Cl^- as compared to inhibitory vesicle populations expressing CLC-3 (Fig. 7c). CLC-3 appears to facilitate inhibitory neurotransmitter loading by providing a shunt conductance to reduce the voltage gradient established by the V-ATPase. Both the expressing and non-CLC-3 expressing inhibitory vesicle populations failed to show a significant Cl^- dependence to the acidification time course. This may reflect the fact that the channel and the V-ATPase work in tandem and the time constant describing activity for the two transport proteins is not significantly different one from the other. CLC-3 activity then enhances the availability of protons at a rate which is consistent with the turnover of the V-ATPase enzyme. It should be noted that the time constants describing acidification in our experiments are on the order of seconds. This is to be compared to the pH-dependent change in fluorescence from Quantum-dots (Q-dots) loaded into synaptic vesicles on the order of 10s of msec 14. The vast difference in time course between the two experimental techniques is likely to be due to the

fact that isolated vesicles in the *in vitro* acidification experiments lack any significant internal Cl^- initially while those vesicles in the Q-dot experiments have high levels of internal Cl^- taken up during the recycling process. Thus, high internal Cl concentrations seem to be highly beneficial in promoting rapid reacidification and, therefore, refilling.

Why does the inhibitory vesicle need to be acidified to fill, since a positive intravesicular potential is not needed to facilitate the influx of the neutral species GABA as is the case with negatively charged glutamate? Two schools of thought have emerged which answer this question postulating two different models of VGAT function. In the recent reconstitution studies of the vesicular inhibitory amino acid transporter, (VIAAT also known as VGAT) of Juge and colleagues 9, VGAT functions as a Cl^- -GABA symporter: GABA enters the vesicle accompanied by two Cl^- ions. The reconstituted studies were carried out using liposomes which did not contain Cl^- initially. In this scenario, the influx of Cl^- driving GABA uptake is a function of the potential gradient set up presumably by the activity of the V-ATPase. What is not clear from the studies of Juge et al. is how the uptake of GABA, and therefore the influx of Cl^-, will change as vesicles recycle; vesicles engulf high Cl^- equal to that in the synaptic cleft following reuptake such that the equilibrium potential for Cl should direct its movement out of the vesicle, inhibiting GABA uptake. The studies of Juge et al. were carried out with liposomes of minimal transporter composition without CLC-3 present. Thus, CLC-3 in native VGAT vesicles may provide a significant parallel efflux pathway clearing the vesicle of high Cl^- concentrations. This allows the transporter, coupled to the Cl^- gradient, to work at maximum rates for rapid refilling during the recycling process. The primary role for CLC-3 in this model would be as an anion efflux pathway maintaining constant transmitter uptake with minimal dependence upon the pH gradient, explaining the competent filling in the absence of acidification.

A competing view of VGAT function holds that the transporter acts as a coupled proton-GABA antiporter. This model is supported by the observation that GABA uptake has a much greater dependence upon the magnitude of the pH gradient (ΔpH) than the voltage gradient (ΔΨ) within the vesicle lumen 16, 19. In this case, increases in luminal Cl^- would shift the energy balance within the vesicle, making ΔpH the principal driving force over the potential gradient (ΔΨ), thus favoring the availability of protons to exchange for GABA in vesicle loading. Our TRIS data support the hypothesis that GABA loading is both dependent upon CLC-3 and pH. TRIS loading reduces inhibitory synaptic transmission more in C*lcn-3*$^{-/-}$ than in *Clcn-3*$^{+/+}$, demonstrating that (1) alkalinization of vesicles reduces GABA loading and (2) that inhibitory vesicles lacking CLC-3 expression are more alkaline than CLC-3 expressing vesicles. Our data favor the VGAT proton-GABA exchanger model in that the exchanger would function when Cl^- concentrations are high in the vesicle lumen during rapid recycling. Furthermore, the expression of CLC-3 would ensure a maximum ΔpH, and hence availability of protons for rapid GABA loading during vesicle recycling at inhibitory synapses in order to maintain rapid firing rates 20, 21.

Our electrophysiological studies demonstrate that not only is quantal size decreased in the *Clcn*$^{-/-}$ neurons but there is also a significant reduction in the frequency of events (Fig. 3b). This could mean that the release probability at the inhibitory synapse is decreased with alkalinized vesicles, something we have observed in capacitance experiments carried out on

Clcn$^{-/-}$ pancreatic beta cells 22 as well as bafilomycin-treated hematopoetic cells in response to secretagogues 23. Vesicle alkalinization has been observed to decrease both the amplitude and frequency of GABAergic mIPSCs in hippocampal slice preparations after treatment with bafilomycin, an effective V-ATPase inhibitor 24. The decrement in vesicle release probability observed following bafilomycin treatment could be due to the release of empty vesicles or alternatively attributed to the fact that vesicle acidification is a necessary prerequisite for release. Unchanged vesicle recycling has been observed in isolated, cultured hippocampal neurons following bafilomycin-treatment using FM1-43 imaging techniques and has been taken as evidence for the hypothesis that vesicle release is independent of the state of vesicle filling or acidification 24. Our data do not distinguish between a scenario in which all vesicles are released with empty vesicles contributing to a decrease in release probability or an alternative scenario in which vesicle release is dependent upon a minimum level of acidification and filling. We cannot rule out the fact that the decrease in the mIPSP frequency which we observe in the *Clcn-3*$^{-/-}$ preparations might be due to the release of vesicles with content low enough so as to make them indistinguishable from baseline noise. Data which would speak against this possibility comes from experiments in Fig. 4 in which TRIS added to the external solution reduced the amplitude of mIPSCs due to the resultant vesicle alkalinization but did not reduce mIPSC frequency. This observation suggests that alkalinization of vesicles alone does not change release probability. The decrement in release frequency seen in the *Clcn-3*$^{-/-}$ slices but not in the TRIS experiments would suggest that CLC-3 expression may facilitate release probability, possibly through an interaction with docking protein machinery. Loss of CLC-3 expression then would bring about the observed decrease in spontaneous release probability.

It is likely that not all inhibitory synapses express CLC-3 presynaptically, considering at least the two major types of perisomatically synapsing interneurons 25. Our data to date do not address this possibility directly but suggest this may be the case since depletion of VGAT-containing vesicles of CLC-3 leaves a significant fraction of vesicles capable of a limited range of acidification. This leaves the intriguing possibility that not all inhibitory vesicles need to acidify to fill or that alternative splice variants of VGAT may be associated with CLC-3 deficient vesicles and function in an unidentified mode. However, it is clear from our investigations that CLC-3, whether transporter or channel in the intracellular compartment, has the capability of enhancing synaptic efficacy via a presynaptic mechanism that regulates synaptic vesicle acidification and filling. Our observations extend the role of Cl^- in inhibitory transmission from that of a postsynaptic permeant species to a presynaptic regulatory element.

Methods

Animals

Studies were performed according to the principles set forth by the Animal Welfare Act and the National Institutes of Health guidelines for the care and use of animals in biomedical research and were approved by the University of Chicago Institutional Animal Care and Use Committee. Adult (8+ weeks) Wistar rats were used in the experiments using isolated synaptic vesicles. In studies examining the impact of CLC-3 expression, we used *Clcn-3*$^{-/-}$

mice (CLC-3 KO) 2 and littermate wild type (WT) mice (*Clcn3*$^{+/+}$) as controls. Genotyping was performed by PCR using REDExtract-N-Amp Tissue PCR Kit (Sigma, St. Louis, MO) and primers specific for the WT allele (forward, 5′-TACATGTTGCCTGCTGCTGT-3′; reverse, 5′-CTGCAGCACTCAACTCCAGA-3′) and also primers specific for the knockout allele (forward, 5′-TGAATGAACTGCAGGACGAG-3′; reverse, 5′-ATACTTTCTCGGCAGGAGCA-3′; as previously described 2, 4.

Antibodies

Two different anti-CLC-3 antibodies were used. Polyclonal rabbit anti-CLC-$3_{730–744}$ was raised against a synthetic peptide corresponding to amino acids 730–744 in the C terminus of a long form of human CLC-3 (Quality Controlled Biochemicals). Specificity of this antibody for CLC-3 has been previously reported 4, 26. Monoclonal anti-CLC-$3_{592–661}$ was raised in mouse against a synthetic peptide corresponding to amino acids 592–661 in rat CLC-3 (Millipore). Mouse monoclonal antibodies against GABA transporter VGAT and glutamate transporter VGLUT1, polyclonal affinity purified antibodies against VGLUT2, vacuolar H^+ transporter V-ATPase and monoclonal antibody against vesicle associated membrane protein VAMP2 were obtained from Synaptic Systems GmbH. Polyclonal guinea pig anti-VGLUT1 antibody was purchased from Sigma. Alexa 488-conjugated goat anti–rabbit and rhodamine-conjugated goat anti-mouse IgG were from Invitrogen. Rhodamine-conjugated rabbit anti-sheep IgG was from ICN. Horseradish peroxidase (HRP)-conjugated goat anti-mouse IgG was purchased from Promega and HRP-conjugated goat anti-rabbit IgG from Pierce. Preimmune rabbit IgG was from Sigma. Goat anti-rabbit IgG conjugated to 15 nm gold particles were obtained from Ted Pella, Inc.

Electrophysiology

Whole-cell voltage-clamp recordings—Whole-cell recordings were made using an EPC9 patch-clamp amplifier (HEKA) and a Multiclamp 700B patch-clamp amplifier (Molecular Devices). Currents were low-pass filtered at 2.8 kHz with an 8-pole Bessel filter and digitized at 10 kHz. Recordings were made from visually identified neurons at +32°C at V_h = −70 mV with an artificial cerebrospinal fluid containing (in mM): 126 NaCl, 2.5 KCl, 1.25 NaH_2PO_4, 26 $NaHCO_3$, 2.5 $CaCl_2$, 1.5 $MgCl_2$ and 10.0 glucose. Miniature IPSCs were recorded in the presence of 1 mM tetrodotoxin (TTX) and 3 mM kynurenic acid added to the bath solution in order to block fast glutamatergic transmission. The patch pipettes were filled with (in mM): 130 CsCl, 1.0 $MgCl_2$, 10.0 HEPES, 0.05 EGTA, 5.0 Mg-ATP, 5.0 QX-314, pH adjusted to 7.3 with CsOH, osmolarity to 288 mOsm. Miniature IPSCs were detected using either MiniAnalysis 6 (Synaptosoft) software or the template search feature for event detection in ClampFit software (pClamp10, Molecular Devices). Both detection schemes gave identical results.

Immunohistochemistry

Tissue Preparation—Mouse brain tissues were intracardially fixed with 4% para-formaldehyde (PFA). Brain tissues were further post-fixed overnight in 4% PFA at 4°C. The excised brain was trimmed to isolate the hippocampal region and was incubated sequentially in 10%, 20%, and 30% sucrose solutions. The hippocampal region was embedded and

frozen in Cryo-O.C.T. compound. Serial cryosections (10 μm thick) were made from the hippocampal block.

Immunostaining—10 μm hippocampal slices were rinsed three times with phosphate-buffered saline (PBS). Slices were permeabilized with Triton X-100 (0.25%) for 5 min. at room temperature. Non-specific binding sites were blocked in PBS containing normal goat serum (5%) and bovine serum albumin (1%). Slices were incubated overnight at 4°C with primary anti-CLC-$3_{592–661}$ (Millipore, 1:100) and polyclonal anti-VGAT (1:200). Primary antibody binding was amplified and visualized with Alexa 488-conjugated goat anti-rabbit antibody (1:500) for anti-CLC3 and Alexa 633-conjugated goat anti-guinea pig antibody (1:500) for anti-VGAT. Coverslips were mounted and observed with a Leica SP5 confocal microscope at 100 × magnification.

Preparation of crude synaptic vesicles (CSV)

The CSV fraction (LP2) was isolated from rat (or mouse) brains as described elsewhere with minor modifications 27. Freshly isolated whole brains were homogenized in an ice-cold homogenization buffer at 3:1 v/w ratio (0.32 M sucrose, 1 mM EGTA in 10 mM HEPES, pH 7.4) containing protease inhibitor cocktail (Sigma) at 1:500 dilution. Cell debris and nuclei were pelleted by centrifugation at 1000 × g. The supernatant was centrifuged at 12,000 × g_{max} for 15 min, resulting in a pellet with two visible layers. The synaptosome-rich upper layer was isolated by gentle resuspension in homogenization buffer followed by centrifugation at 13,000 × g_{max} for 15 min to obtain crude synaptosomes. To release synaptic vesicles from synaptosomes, the pellet was subjected to a hypotonic lysis and immediately homogenized with three strokes in a homogenizer. To this homogenate, 1 M HEPES, pH 7.4 with protease inhibitors was added to a final concentration of 7.5 mM. The lysate was centrifuged at 33,000 × g_{max} for 20 min, yielding a supernatant containing synaptic vesicles and a pellet containing lysed synaptosomal membranes. The supernatant was centrifuged at 225,000 × g_{max} for 2 hr. The resultant pellet (LP2 fraction) containing crude synaptic vesicles (CSV) was suspended in homogenization buffer and used immediately.

For studies examining the role of CLC-3 in synaptic vesicle acidification, it was critical to carry out the isolation in an expedited manner since CLC-3 is known to be highly sensitive to degradation. Therefore, we sacrificed CVS fraction purity in order to preserve CLC-3 function and did not do lengthy purification of CVS on a controlled pore glass chromatography column. Additionally, in that CLC-3 functionality was lost during freeze thaw, acidification of vesicles was only performed on freshly isolated preparations.

All centrifugations were carried out at 4°C. The quality/homogeneity of the preparation was verified by electron microscopy.

Immuno-isolation of synaptic vesicle subpopulations for acidification assay by negative selection

The subpopulations of synaptic vesicles were isolated using CELLection™ Biotin Binder kit (Invitrogen Dynal AS). The magnetic beads coated with streptavidin were conjugated to

biotinylated anti-VGLUT1 or anti-VGAT antibodies (Synaptic Systems) and incubated with (LP2) fraction for 2 hrs at 4°C in order to deplete crude synaptic vesicles of excitatory (VGLUT1-positive) or inhibitory (VGAT-positive) synaptic vesicle subpopulations, respectively. Beads associated with VGLUT1- or VGAT-positive synaptic vesicles were removed from the suspension magnetically. The degree of depletion was characterized by Western blotting. VGLUT1- and VGAT-depleted synaptic vesicle subpopulations are referred to as “inhibitory” and “excitatory”, respectively. In experiments investigating the role of CLC-3 in acidification of inhibitory synaptic vesicles, the inhibitory synaptic vesicles were further depleted of CLC-3 by incubation with magnetic beads conjugated to anti-CLC-3 antibody. The beads with attached CLC-3-positive synaptic vesicles were removed from the suspension magnetically and the degree of depletion was confirmed by Western blot.

Immuno-isolation of inhibitory synaptic vesicles by positive selection for electron microscopy

Inhibitory synaptic vesicles were isolated from LP2 fraction on Sphero™ amino-polystyrene microparticles (Spherotech, Inc.), 1 μm in diameter. Anti-VGAT was covalently linked to the microbeads using (1-ethyl-3(-3-dimethylaminopropyl) carbodiimide hydrochloride) (EDC) (Sigma) as a coupling agent according to a manufacturer’s protocol. CSV suspension was incubated with the beads for 2 hours at 4°C. The beads with attached VGAT-positive synaptic vesicles were pelleted by centrifugation at 3,000 × g and washed 3 times in PBS.

Western blotting of synaptic vesicle preparations

Preparations of synaptic vesicles were solubilized in Laemmli sample buffer. Aliquots were taken for protein determination by BCA assay (Pierce, Thermo Scientific), after which dithiothreitol (DTT; 50 mM) was added. Samples were heated at 65°C for 15 min since boiling often results in formation of higher molecular mass complexes by CLC-3. Proteins were resolved by SDS-PAGE on gradient 4–20% gels and transferred to a PVDF membrane. Blots were incubated for 1 hr at room temperature or overnight at 4°C with anti-VGLUT1 (1:100,000), anti-VGAT (1:500), or anti-CLC-3 (1:200) and subsequently with goat anti-mouse (Promega) or goat anti-rabbit (Pierce), secondary antibodies (1:10,000) conjugated to horseradish peroxidase. Preimmune rabbit or mouse IgG (Sigma) was used as a negative control. Detection was performed using Super Signal® West Dura Extended Duration Substrate (Pierce, Thermo Scientific). The staining was visualized using the SYNGENE Bioimaging System (Synoptics LTD).

Localization of CLC-3 on VGAT-positive synaptic vesicles by immuno – electronmicroscopy

Microbeads (Spherotech, Inc.) with attached VGAT-positive synaptic vesicles were pelleted by centrifugation, and the pellet was fixed with 0.15% glutaraldehyde and 4% paraformaldehyde for 1 hr at 4°C, washed with PBS, and embedded in LR white resin (Electron Microscopy Science) at 45°C in a vacuum oven for 48 hr. Preparations were sectioned (90 nm) with a Reichert-Jung Ultracut E microtome. Sections were stained with anti-CLC-$3_{730–744}$ (1:100). Preimmune rabbit IgG (Sigma) was used as a negative control.

CLC-3 was visualized using goat anti-rabbit antibodies conjugated to 15 nm gold particles. Images were captured using a Tecnai F30 transmission electron microscope (TEI).

Acidification of synaptic vesicles

Acridine orange, a pH-sensitive dye, was used as an indicator to evaluate acidification of synaptic vesicles. Changes in fluorescence were measured with spectrofluorometer FluoroMax 3 (Horiba Jobin Yvon) using excitation at 492 nm and emission at 528 nm 28 at a time increment 0.5 sec. Synaptic vesicles (25–50 μg) were resuspended in 10 mM 3-[N-morpholino]propanesulfonic acid (MOPS)-CsOH with 320 mM sucrose and 4 mM $MgSO_4$, pH 7.4 and equilibrated at 32°C. Final reaction volume was 1 ml and contained 1 μM acridine orange, 2 mM ATP to initiate acidification, 10 mM neurotransmitter when indicated (either GABA or glutamate) and varying Cl^- concentrations (0, 5, 35, 80 and 150 mM choline chloride). The reaction was performed with identical protein amounts of all fractions at constant mixing with a magnetic stirrer. In order to isolate the effect of $[Cl^-]$ on acidification, the buffer was devoid of K^+ and Na^+. A protonophore carbonyl cyanide 4-(trifluoromethoxy) phenylhydrazone (FCCP) at 40 μM was added at the end of reaction to equalize the intravesicular pH with that of the medium. High reproducibility of this methodology in our preparations can be seen on Supplemental Fig. 3.

Data analysis and miscellaneous procedures

All data in this study, unless otherwise indicated represents mean values ± S.E.M. with the number of trials, cells or animals in parentheses. Synaptic vesicle studies represent means from at least three different preparations. Confidence was assessed by either two-tailed unpaired Student's t test between data sets or one way ANOVA using Origin Pro 8.2 (Northhampton, MA) or PCLAMP (Molecular Devices, CA) software as indicated in the figure legends. The time constant (τ) for synaptic vesicle acidification was determined from single exponential fits to the fluorescence data using Origin Pro 8.2 software. Multi-peak Gaussian fits to the mIPSC data was used to derive mean center peaks used in the analysis in Fig. 3D.

Supplementary Material

Refer to Web version on PubMed Central for supplementary material.

ACKNOWLEDGMENTS

The authors wish to express their appreciation to Drs. Aaron Fox, Shigeo Takamori, Robert Edwards, Laurel Farmer and Radmila Sarac for many helpful conversations during the course of the work; Dr. Vytautas Bindokas for technical help with immunostaining; Yimei Chen for help with the immuno-electron microscopy; and to Dr. Fred Lamb at the University of Iowa who provided the $Clcn^{-/-}$ strain. The study was supported by NIH R01 GM36823 and NIH R01 DK 080364 to D.J.N.

REFERENCES

1. Stobrawa SM, et al. Disruption of ClC-3, a chloride channel expressed on synaptic vesicles, leads to a loss of the hippocampus. Neuron. 2001; 29:185–196. [PubMed: 11182090]

2. Dickerson LW, et al. Altered GABAergic function accompanies hippocampal degeneration in mice lacking ClC-3 voltage-gated chloride channels. Brain Res. 2002; 958:227–250. [PubMed: 12470859]
3. Yoshikawa M, et al. CLC-3 deficiency leads to phenotypes similar to human neuronal ceroid lipofuscinosis. Genes Cells. 2002; 7:597–605. [PubMed: 12059962]
4. Wang XQ, et al. CLC-3 channels modulate excitatory synaptic transmission in hippocampal neurons. Neuron. 2006; 52:321–333. [PubMed: 17046694]
5. Maritzen T, Keating DJ, Neagoe I, Zdebik AA, Jentsch TJ. Role of the vesicular chloride transporter ClC-3 in neuroendocrine tissue. J Neurosci. 2008; 28:10587–10598. [PubMed: 18923035]
6. Schenck S, Wojcik SM, Brose N, Takamori S. A chloride conductance in VGLUT1 underlies maximal glutamate loading into synaptic vesicles. Nat Neurosci. 2009; 12:156–162. [PubMed: 19169251]
7. Habela CW, Olsen ML, Sontheimer H. ClC3 is a critical regulator of the cell cycle in normal and malignant glial cells. J Neurosci. 2008; 28:9205–9217. [PubMed: 18784301]
8. Cuddapah VA, Sontheimer H. Molecular interaction and functional regulation of ClC-3 by Ca2+/calmodulin-dependent protein kinase II (CaMKII) in human malignant glioma. The Journal of biological chemistry. 285:11188–11196. [PubMed: 20139089]
9. Juge N, Muroyama A, Hiasa M, Omote H, Moriyama Y. Vesicular inhibitory amino acid transporter is a Cl-/gamma-aminobutyrate Co-transporter. The Journal of biological chemistry. 2009; 284:35073–35078. [PubMed: 19843525]
10. Gulyas AI, Megias M, Emri Z, Freund TF. Total number and ratio of excitatory and inhibitory synapses converging onto single interneurons of different types in the CA1 area of the rat hippocampus. J Neurosci. 1999; 19:10082–10097. [PubMed: 10559416]
11. Takamori S, Riedel D, Jahn R. Immunoisolation of GABA-specific synaptic vesicles defines a functionally distinct subset of synaptic vesicles. J Neurosci. 2000; 20:4904–4911. [PubMed: 10864948]
12. Atluri PP, Ryan TA. The kinetics of synaptic vesicle reacidification at hippocampal nerve terminals. J Neurosci. 2006; 26:2313–2320. [PubMed: 16495458]
13. Gandhi SP, Stevens CF. Three modes of synaptic vesicular recycling revealed by single-vesicle imaging. Nature. 2003; 423:607–613. [PubMed: 12789331]
14. Zhang Q, Cao YQ, Tsien RW. Quantum dots provide an optical signal specific to full collapse fusion of synaptic vesicles. Proceedings of the National Academy of Sciences of the United States of America. 2007; 104:17843–17848. [PubMed: 17968015]
15. Kerr AM, Reisinger E, Jonas P. Differential dependence of phasic transmitter release on synaptotagmin 1 at GABAergic and glutamatergic hippocampal synapses. Proceedings of the National Academy of Sciences of the United States of America. 2008; 105:15581–15586. [PubMed: 18832148]
16. Edwards RH. The neurotransmitter cycle and quantal size. Neuron. 2007; 55:835–858. [PubMed: 17880890]
17. Hnasko TS, et al. Vesicular glutamate transport promotes dopamine storage and glutamate corelease in vivo. Neuron. 65:643–656. [PubMed: 20223200]
18. Gronborg M, et al. Quantitative comparison of glutamatergic and GABAergic synaptic vesicles unveils selectivity for few proteins including MAL2, a novel synaptic vesicle protein. J Neurosci. 30:2–12. [PubMed: 20053882]
19. Hell JW, Maycox PR, Jahn R. Energy dependence and functional reconstitution of the gamma-aminobutyric acid carrier from synaptic vesicles. The Journal of biological chemistry. 1990; 265:2111–2117. [PubMed: 1688846]
20. Kraushaar U, Jonas P. Efficacy and stability of quantal GABA release at a hippocampal interneuron-principal neuron synapse. J Neurosci. 2000; 20:5594–5607. [PubMed: 10908596]
21. Bartos M, Vida I, Frotscher M, Geiger JR, Jonas P. Rapid signaling at inhibitory synapses in a dentate gyrus interneuron network. J Neurosci. 2001; 21:2687–2698. [PubMed: 11306622]
22. Deriy LV, et al. The granular chloride channel ClC-3 is permissive for insulin secretion. Cell metabolism. 2009; 10:316–323. [PubMed: 19808024]

23. Deriy LV, et al. Disease-causing mutations in the cystic fibrosis transmembrane conductance regulator determine the functional responses of alveolar macrophages. The Journal of biological chemistry. 2009; 284:35926–35938. [PubMed: 19837664]

24. Zhou Q, Petersen CC, Nicoll RA. Effects of reduced vesicular filling on synaptic transmission in rat hippocampal neurones. The Journal of physiology. 2000; 525(Pt 1):195–206. [PubMed: 10811737]

25. Klausberger T, Somogyi P. Neuronal diversity and temporal dynamics: the unity of hippocampal circuit operations. Science (New York, N.Y. 2008; 321:53–57.

26. Huang P, et al. Regulation of human CLC-3 channels by multifunctional Ca2+/calmodulin-dependent protein kinase. The Journal of biological chemistry. 2001; 276:20093–20100. [PubMed: 11274166]

27. Hell, JW.; Jahn, R. Cell Biology. A Laboratory Handbook. Celis, JE., editor. Vol. Vol. 1. San Diego: Academic Press, Inc.; 1994. p. 567-574.

28. Maycox PR, Deckwerth T, Hell JW, Jahn R. Glutamate uptake by brain synaptic vesicles. Energy dependence of transport and functional reconstitution in proteoliposomes. The Journal of biological chemistry. 1988; 263:15423–15428. [PubMed: 2902091]

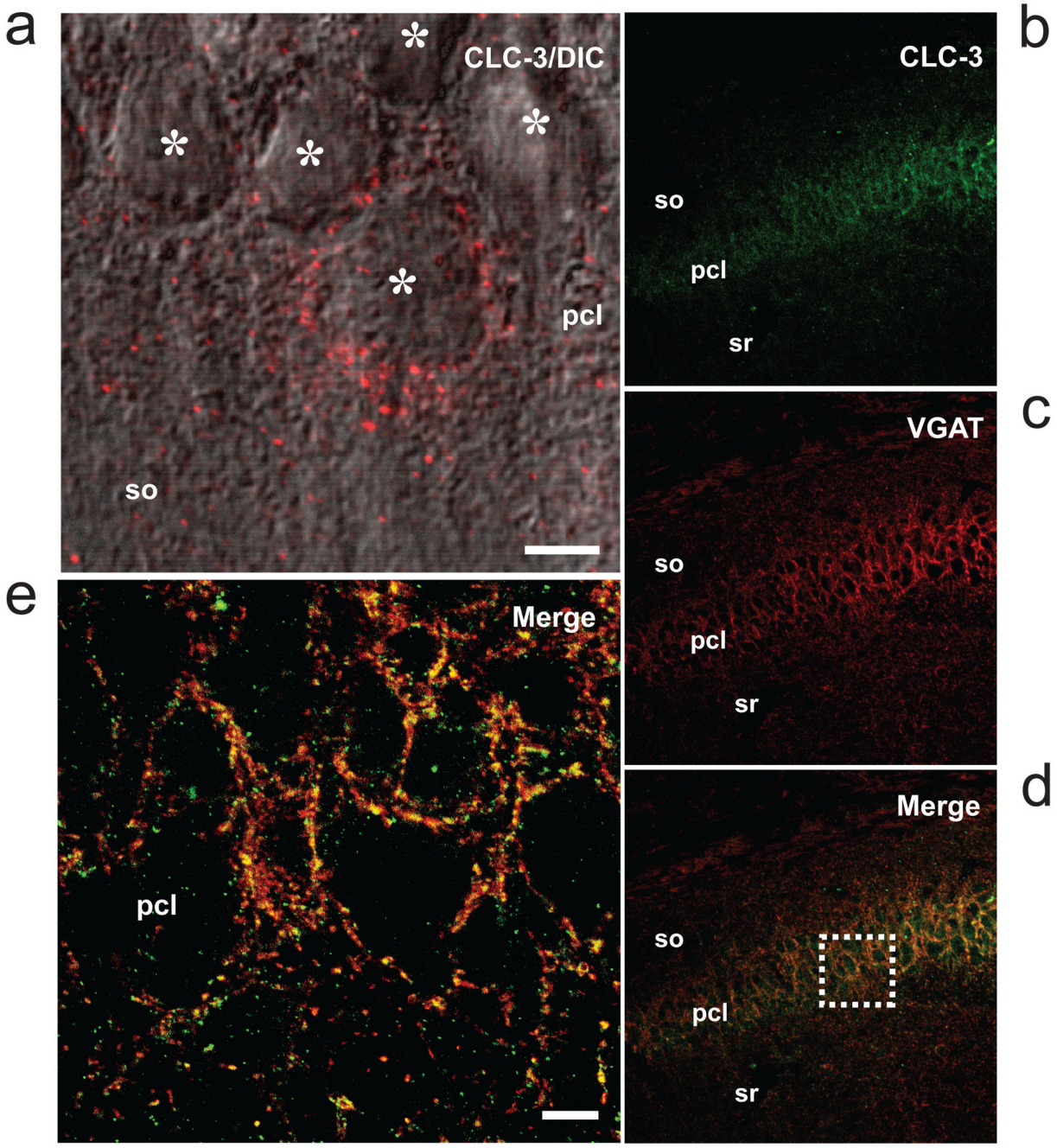

Figure 1. CLC-3 colocalization with VGAT

Immunofluorescent labeling of the CLC-3 in CA1 area of hippocampus. (**a**) DIC image and fluorescent immunostaining for CLC-3 (red dots) show perisomatic localization of CLC-3 around CA1 pyramidal cell bodies (*). Calibration bar represents 5 μm. (**b–d**). Double immunostaining with anti-CLC-$3_{730–744}$ (green) and anti-VGAT antibody (red) in the CA1 region reveals prominent co-localization of CLC-3 with the vesicular GABA transporter in the CA1 pyramidal cell layer (pcl). (**e**) Enlarged image (taken from boxed area in (**d**) specifies their co-localization to a subset of puncta adjacent to cell bodies of pyramidal

neurons. Qualitative analysis of colocalization was done using ImageJ plug-in Jacop. Background subtraction was performed to eliminate noise. Spots analyzed were plotted as the normalized intensity of CLC-3 (green) as a function of VGAT (red). Manders' Coefficients (with threshold) were 0.44 for fraction of VGAT overlapping ClC-3 and 0.8 for the fraction of CLC-3 overlapping VGAT with an overlap correlation coefficient of 0.92. Calibration bar represents 10 μm. *Stratum radiatum* = sr, pyramidal cell layer = pcl, and *stratum oriens* = so.

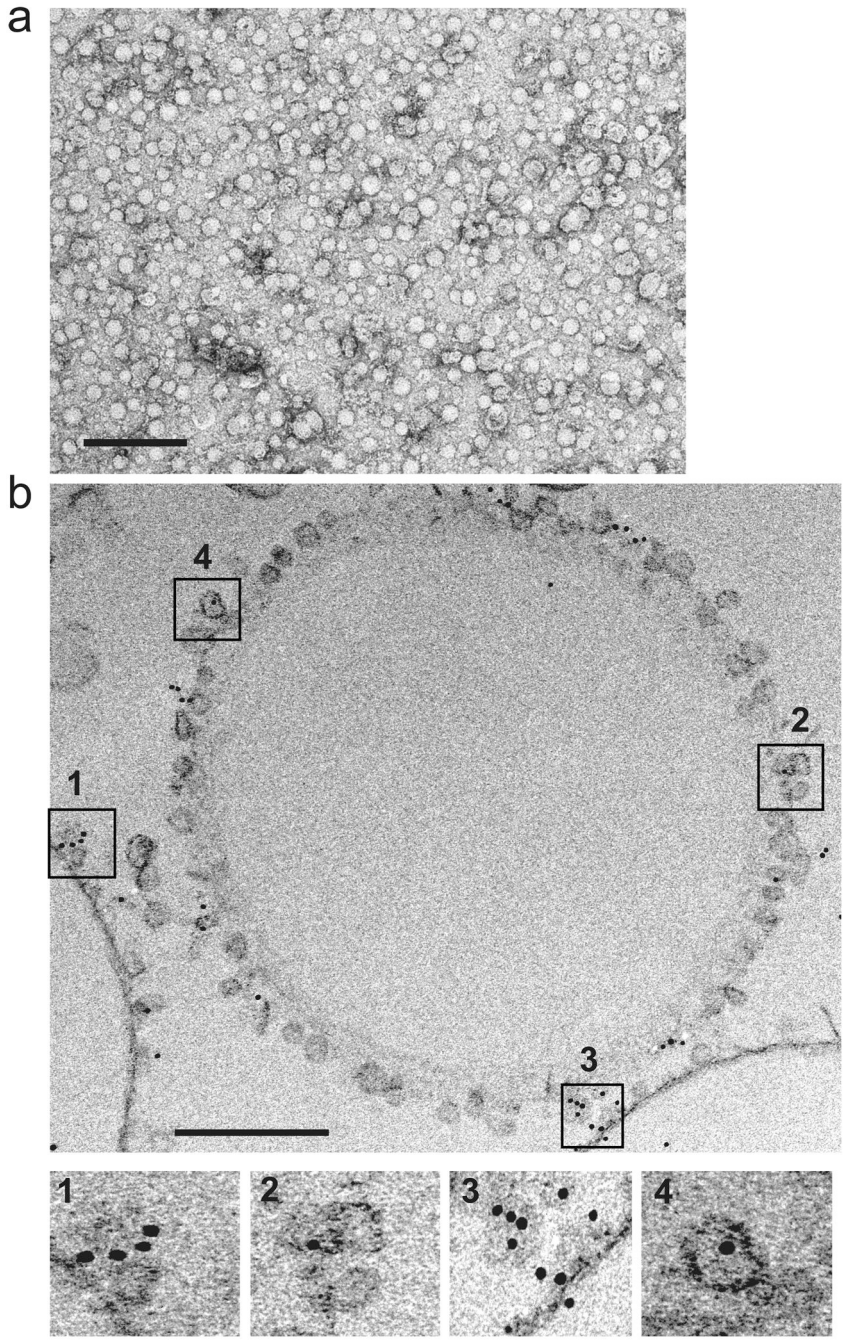

Figure 2. Immunogold localization of CLC-3 on inhibitory synaptic vesicle fractions

(**a**) Electron micrograph of crude CSV fraction (LP2) purified as described in Methods. This fraction served as a starting material for immunoisolation of subsets of synaptic vesicles. Scale bar represents 200 nm. (**b**) Electron micrograph of CLC-3 immuno-detection on immuno-isolated inhibitory synaptic vesicles. Monoclonal VGAT antibody was conjugated to *Spherobeads* (diameter = 1–1.4 μm) and used for positive selection of inhibitory synaptic vesicles followed by post-embedding staining with anti-CLC-3 antibody and secondary goat

anti-rabbit IgG conjugated to 15 nm gold particles. Scale bar represents 200 nm. Lower panel: Corresponding enlargements of boxed areas in (**b**) above.

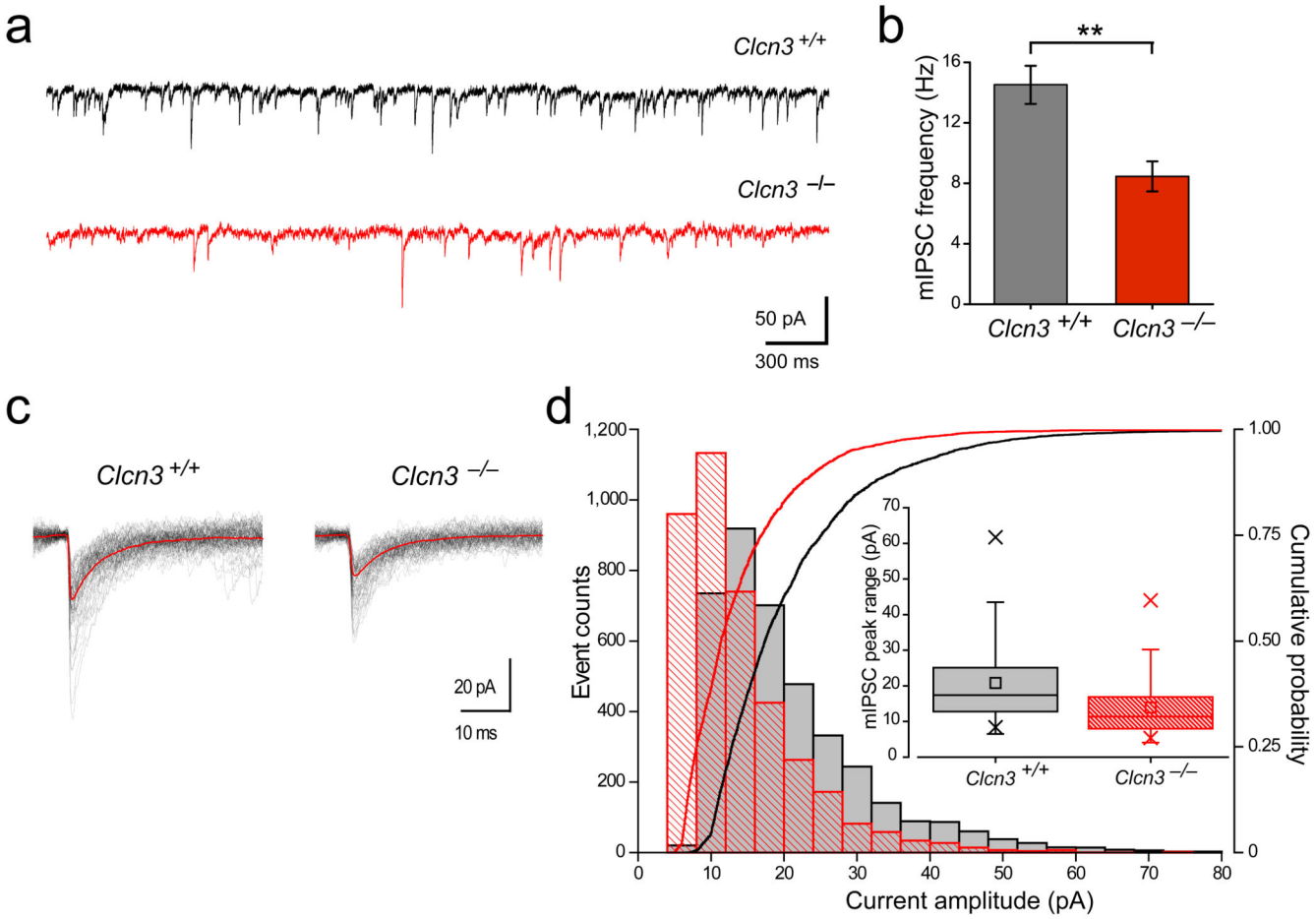

Figure 3. Decreased miniature IPSC frequency and amplitudes in *Clcn3*$^{-/-}$ mice

(**a**) Representative miniature IPSCs (mIPSCs) traces recorded in the presence of TTX (1 μM) and kynurenic acid (3 mM) from a CA1 pyramidal neuron from *Clcn3*$^{+/+}$ and *Clcn3*$^{-/-}$ preparations. (**b**) Data summary demonstrating a significant decrease in IPSC frequency in *Clcn3*$^{-/-}$ neurons (*Clcn3*$^{+/+}$ 14 ± 1.3 Hz, n = 13 cells; *Clcn3*$^{-/-}$ 8.4 ± 1.0 Hz, n = 9 cells, (**$P < 0.005$ One way ANOVA). (**c**) Representative detected and superimposed mIPSC traces recorded from CA1 pyramidal cells in *Clcn3*$^{+/+}$ and *Clcn3*$^{-/-}$ slices. Average current traces are shown by the smooth red line. (**d**) Cumulative amplitude distribution of mIPSCs recorded from *Clcn3*$^{+/+}$ (filled gray bars) *and Clcn3*$^{-/-}$ (hatched red bars) neurons; 3934 events from 7 cells were used for analysis for each group. Superimposed cumulative amplitude probability graph of mIPSCs from *Clcn3*$^{+/+}$ (black line) and *Clcn3*$^{-/-}$ (red line) neurons shows that amplitude distribution is shifted to the left for the *Clcn3*$^{-/-}$ events indicating smaller mIPSCs in the *Clcn3*$^{-/-}$ mice ($P < 0.001$ Kolmogorov-Smirnov test). Insert: Box plot analysis of average amplitude of mIPSCs from *Clcn3*$^{+/+}$ (black) and *Clcn3*$^{-/-}$ (red) neurons.

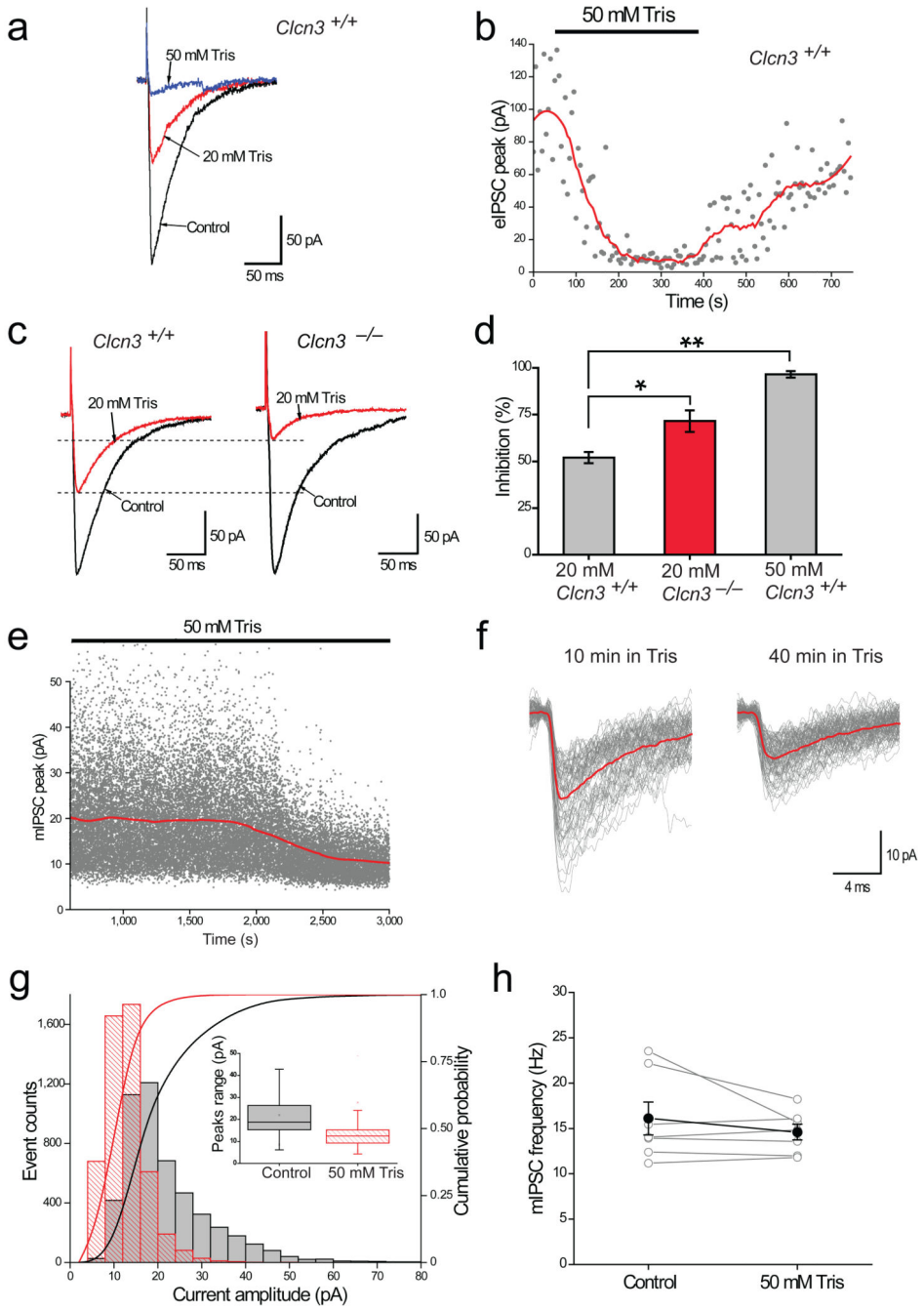

Figure 4. Buffering with TRIS reduces inhibitory synaptic transmission

(**a**) Representative evoked IPSC traces recorded before (black line) and during extracellular application of 20 mM (red trace) and 50 mM (blue trace) of TRIS. (**b**) Time course of evoked IPSC peak amplitude changes with bath application of 50 mM TRIS (pH 7.4) during 0.2 Hz stimulation. Average of every 10 eIPSC peaks is shown by the smooth red line. (**c**) Representative evoked IPSC traces recorded before (black line) and during extracellular application of 20 mM (red trace) of TRIS from a representative CA1 pyramidal neuron from the *Clcn3*$^{+/+}$ and *Clcn3*$^{-/-}$ animals. (**d**) Pooled data showing significantly different (*P <

0.05, $^{**}P < 0.005$ one-way ANOVA) inhibition of evoked IPSCs with 20 mM TRIS in slices from *Clcn3*$^{+/+}$ (n = 7) and *Clcn3*$^{-/-}$ (n = 5) animals and 50 mM (n = 6) TRIS in slices from *Clcn3*$^{+/+}$ animals. (**e**) Representative time course of miniature IPSC peak amplitude (grey dots) changes with bath application of 50 mM TRIS (pH 7.4). Average of every 10,000 mIPSC peaks is shown by the smooth red line. (**f**) Representative detected and superimposed mIPSC traces recorded from a CA1 pyramidal cell in *Clcn3*$^{+/+}$ slice at 10 min and 40 min of recording in 50 mM TRIS. Average current traces are shown by the smooth red line. (**g**) Cumulative amplitude distribution of mIPSCs recorded before (filled gray bars) and 30 min after (hatched red bars) perfusion *Clcn3*$^{+/+}$ slices with 50 mM TRIS; 6,000 events from 6 cells were used for analysis for each group. Cumulative amplitude probability graph of mIPSCs peaks during control (black line) and 50 mM TRIS (red line) from *Clcn3*$^{+/+}$ neurons shows that the amplitude distribution is shifted to the left for events recorded in TRIS indicating smaller mIPSC sizes ($P < 0.001$ Kolmogorov-Smirnov test). Insert: Box plot analysis of average amplitude of mIPSCs in control period (black) and period with TRIS effect (red) on mIPSC. (**h**) Data summary demonstrating changes in mIPSC frequency in control period and 30 min after 50 mM TRIS application (Control period: 16.1 ± 1.8 Hz, 30 min in TRIS: 14.6 ± 0.9 Hz, n = 7 cells).

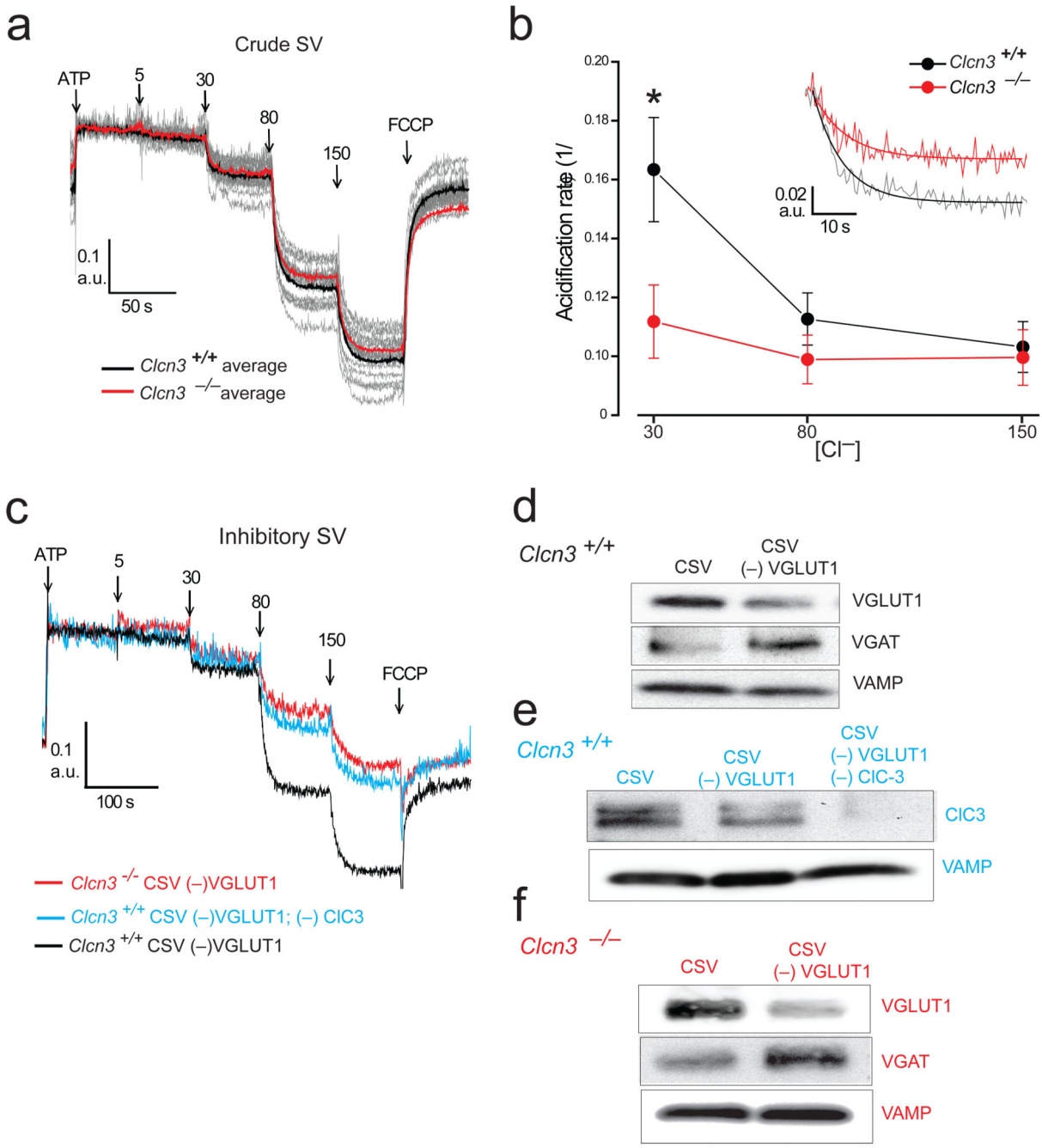

Figure 5. Immunoisolation reveals importance of CLC-3 for acidification of inhibitory synaptic vesicles

(**a**) Averaged traces of [Cl^-]-dependent acidification of CSV obtained from *Clcn3*$^{+/+}$ (black, n = 10) and *Clcn3*$^{-/-}$ (red, n = 9) mice normalized against the original level of acridine orange fluorescence at 2 mM ATP and 0 mM Cl^-. (**b**) Effect of CLC-3 on the rates of acidification of *Clcn3*$^{+/+}$ versus *Clcn3*$^{-/-}$ CSV calculated as tau of decay from exponential fits of individual traces. Data are presented as a mean ± standard error, *Clcn3*$^{+/+}$ (black, n = 10) and *Clcn3*$^{-/-}$, (red, n = 9); (*$P < 0.05$ one-way ANOVA). Insert: Exponential fits of

individual acidification traces at a single Cl^- concentration as an example of differential effect of CLC-3 on the rate of acidification of *Clcn3*$^{+/+}$ versus *Clcn3*$^{-/-}$ CSV. (**c**) Importance of CLC-3 for the degree of acidification of inhibitory synaptic vesicles demonstrated by representative traces of acidification of inhibitory synaptic vesicle (CSV(−)VGLUT1) from *Clcn3*$^{-/-}$ (red), *Clcn3*$^{+/+}$ (black) and *Clcn3*$^{+/+}$ CLC-3-depleted (blue) synaptic vesicles. Traces represent preparations each consisting of at least 8 animals. (**d–f**) Western blot characterization of immunoisolated fractions of synaptic vesicles obtained from *Clcn3*$^{+/+}$ and *Clcn3*$^{-/-}$ mice. (**d**) Upper panel: blot probed with anti-VGLUT1 antibody to show the depletion of VGLUT1 (CSV(−)VGLUT1). Middle panel: probed with anti-VGAT antibody to show VGAT enrichment of (CSV(−)VGLUT1) fraction. Lower panel: probed with anti-VAMP antibody as a load control. (**e**) Western blot of doubly depleted fraction probed with anti-CLC-3 (upper panel) shows that CSV(−)VGLUT1(−)CLC-3 fraction is in fact devoid of CLC-3. Anti-VAMP detection was used as a load control (lower panel). (**f**) Characterization of VGLUT1 depletion (upper panel) and VGAT enrichment (middle panel) of SV immunoisolated from *Clcn3*$^{-/-}$ mouse. Anti-VAMP detection was performed to control for loading of the lanes. For full-length blots, see Supplementary Figure 5.

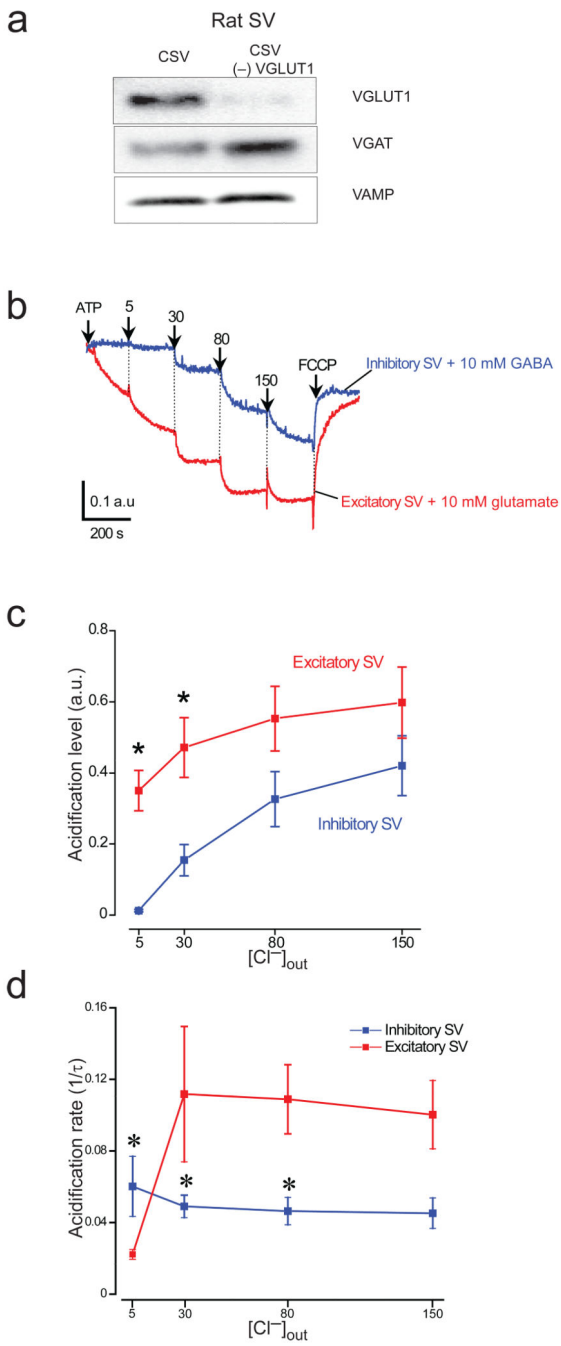

Figure 6. Differential degree and rate of acidification of inhibitory versus excitatory synaptic vesicles

(**a**) Western blot characterization of rat enriched inhibitory synaptic vesicle fraction immuno-isolated by depletion on magnetic beads coated with anti-VGLUT1 antibodies (see Methods). Upper panel: blot probed with anti-VGLUT1 antibody to show the depletion of VGLUT1 (CSV(−)VGLUT1). Middle panel: probed with anti-VGAT antibody to show VGAT enrichment of (CSV(−)VGLUT1) fraction. Lower panel: probed with anti-VAMP antibody as a load control. (**b**) Representative traces of acidification in arbitrary fluorescence units (a.u.) of inhibitory (CSV(−)VGLUT1) and excitatory (CSV(−)VGAT) synaptic

vesicles as a function of various Cl^- concentrations and in the presence of 10 mM GABA or glutamate, respectively. (**c**) Comparison of the degree of [Cl^-]-dependent acidification (in arbitrary units) calculated as the fraction of the initial level of acridine orange fluorescence at 2 mM ATP and 0 mM Cl^- in inhibitory (blue) vs. excitatory (red) synaptic vesicle fractions in the presence of 10 mM of GABA or glutamate, respectively. (**d**) Comparison of the rate of [Cl^-]-dependent acidification in inhibitory (blue) and excitatory (red) synaptic vesicle fractions calculated as the decay time constant (τ) determined from exponential fits to individual traces. Data in **c** and **d** are presented as the mean ± standard error (n = 3), (*P < 0.05 one-way ANOVA). N represents a number of preparations each consisting of at least 5 animals. For full-length blots, see Supplementary Figure 6.

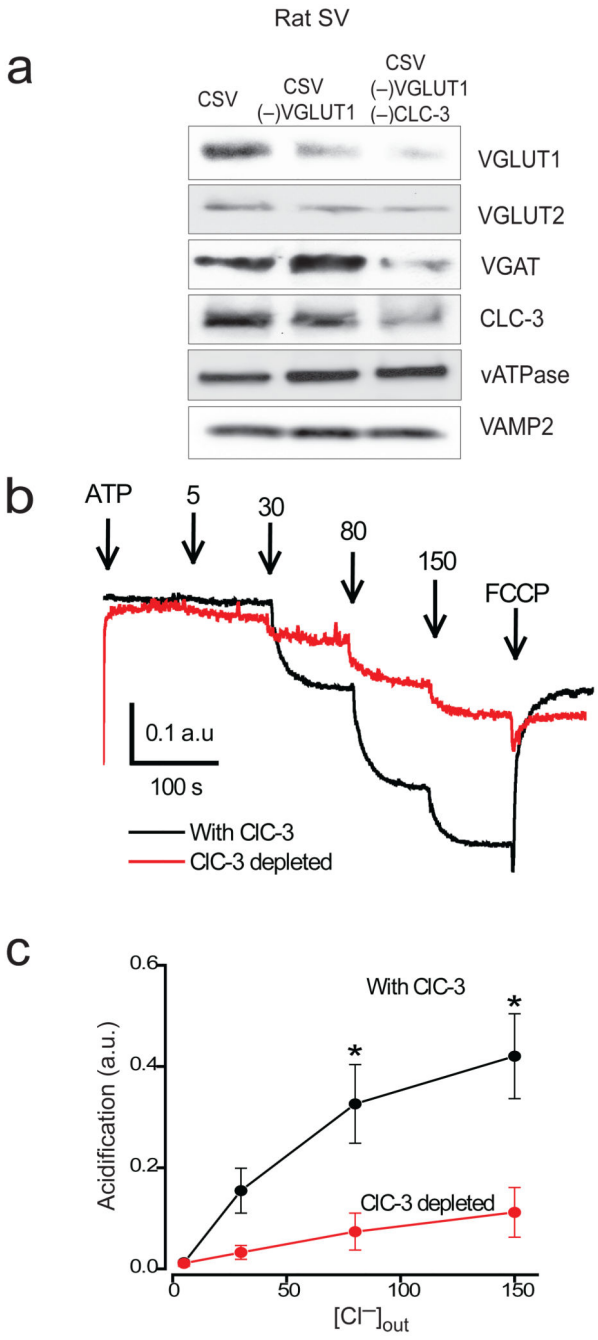

Figure 7. CLC-3 is important for the degree and the rate of acidification of inhibitory synaptic vesicles

(**a**) Western blot characterization of CSVs, inhibitory synaptic vesicle fraction (CSV(−)VGLUT1) and inhibitory synaptic vesicle fraction depleted of CLC-3 on magnetic beads coated with anti-CLC-3 (CSV(−)VGLUT1(−)CLC-3). Western blot was probed with antibodies against VGLUT1, VGLUT2, VGAT, CLC-3 and vATPase. Blot probed with anti-VAMP2 antibody served as a load control. (**b**) Representative traces of [Cl^-]-dependent acidification for inhibitory synaptic vesicles in the presence (black) or absence (red) of

CLC-3. Acidification was initiated by addition of 2 mM ATP in the presence of 10 mM GABA. (**c**) Comparison of levels of [Cl^-]-dependent acidification of inhibitory synaptic vesicles in the presence (black) or absence (red) of CLC-3 calculated as a fraction of the original level at 2 mM ATP and 0 mM Cl^-. For full-length blots, see Supplementary Figure 7.